High magnetic field study of lattice and magnetic effects on the charge-melting transition in $L_{1/2}Ca_{1/2}MnO_3$ perovskites

M. Respaud
LPMC, SNCMP, INSA Complexe Scientifique de Rangueil, F-31077 Toulouse, France
and Institut de Ciència de Materials de Barcelona, Consejo Superior de Investigaciones Científicas, Campus Universitat Autònoma de Barcelona, Bellaterra 08193, Spain

A. Llobet
Institut de Ciència de Materials de Barcelona, Consejo Superior de Investigaciones Científicas, Campus Universitat Autònoma de Barcelona, Bellaterra 08193, Spain
and Laboratoire Louis Néel, CNRS, BP 166, F-38042 Grenoble Cedex, France

C. Frontera
Institut de Ciència de Materials de Barcelona, Consejo Superior de Investigaciones Científicas, Campus Universitat Autònoma de Barcelona, Bellaterra 08193, Spain

C. Ritter
Institut Laue-Langevin, F-38042 Grenoble Cedex, France

J. M. Broto, H. Rakoto, and M. Goiran
LPMC, SNCMP, INSA Complexe Scientifique de Rangueil, F-31077 Toulouse, France

J. L. García-Muñoz
Institut de Ciència de Materials de Barcelona, Consejo Superior de Investigaciones Cientificas, Campus Universitat Autònoma de Barcelona, Bellaterra 08193, Spain
(Received 11 August 1999)

Pulsed magnetic fields up to 50 T and neutron-diffraction measurements have been used in a systematic investigation of the lattice and magnetic factors contributing to the charge-melting transition in $L_{1/2}Ca_{1/2}MnO_3$ perovskites (L:Y→La). A detailed study of the *H-T* phase diagrams is presented. The remarkable rising of the critical fields (nonlinear) contrasts with the evolution of the transition temperatures. Possible factors determining the evolution observed under field are discussed in the light of the experimental data.

I. INTRODUCTION

Over the past few years great interest has been focused on the charge and orbital ordering phenomena in doped manganese $L_{1-x}(Ca, Sr)_xMnO_3$ (Ref. 1) or $La_{1-x}Sr_{1+x}MnO_4$ (Ref. 2) and nickel $La_{2-x}Sr_xNiO_4$ (Ref. 3) perovskites. The formation of periodic patterns with polaron ordering is being intensively studied in mixed valence manganites, where electron-lattice correlations play an essential role. A commensurate fraction of the carrier concentration favors long-range ionic ordering of Mn^{3+} and Mn^{4+} ions. Simultaneous orbital ordering has been reported to accompany the charge-ordering (CO) transitions in these oxides. In most of the cases, this transition occurs well above the antiferromagnetic (AFM) ordering of the Mn spins.[4,5] Given that the localized e_g charges (Mn^{3+} sites) induce local lattice distortions [Jahn-Teller (JT) deformation], the interplay between the charge and orbital ordering tries to minimize the lattice energy of the new periodic pattern.

The observation that charge and orbital ordered states can be disrupted under application of external fields is stimulating intense work, aimed at examining the structural, magnetic, and electronic transitions induced under field. In the magnetic-field-melting mechanism the induced polarization of the electronic spins competes with the trapping of the charges and favors their delocalization. The temperature-field phase diagram for the ferromagnetic (FM) metal to AFM nonmetal transition of $Pr_{1/2}Sr_{1/2}MnO_3$ was published in Ref. 6. A systematic study of the metal-insulator (M-I) phase diagram in the *H-T* plane was reported by Tokura *et al.* in Ref. 7 and Kuwahara *et al.* in Ref. 8 for the $(Nd_{1-y}Sm_y)_{1/2}Sr_{1/2}MnO_3$ series. In this series of crystals with small Mn-O-Mn distortion, an undercooled ferromagnetic (FM) metallic state was found to compete with the CO state at low temperatures and small fields. Moreover, $L_{1-x}Ca_xMnO_3$ crystals (L=Pr and Nd) with $x=0.4-0.56$ were investigated under high fields in Refs. 9, 10, and 11, where it was confirmed that the robustness of the CO phase at 4.2 K strongly depends on the rare earth and the carrier concentration. Of special interest was the temperature dependence of the critical fields in samples with a discommensurate CO state and a significant distortion. The positive dH_c/dT dependence of $Pr_{1-x}Ca_xMnO_3$ ($1/3 \leqslant x < 1/2$), for instance, was ascribed to entropic effects due to the excess of e_g electrons.[9]

With the objective of contributing to a more precise description and understanding of the melting of ordered polarons in the most stable CO case ($x=1/2$), we have per-

formed a systematic study on $L_{1/2}Ca_{1/2}MnO_3$ perovskites with L=Y, Ho, Sm, Nd, Pr, and La. For the present study we chose the L-Ca series, without Sr, for two reasons. (i) First, in order to minimize the effects coming from the radii distribution at the L site. The radius of the Ca^{2+} cation is rather similar to the radius of the lanthanides investigated and much smaller than the Sr^{2+} radius. (ii) The real ground state of $L_{1/2}Sr_{1/2}MnO_3$ compounds have been recently revised, after the confirmation that their orbital ordering does not correspond to a CO state but they are two-dimensional metallic antiferromagnets.[12] In general, the charge-ordered state in most of the 50% Sr-doped perovskites is rather fragile. A very slight deviation of the 50% stoichiometry is enough to destroy the charge-ordered state. By decreasing the temperature, reversible phase separation phenomena are commonly found, and metastable reentrant states are easily found at low temperatures in samples with a distribution of atomic radius at the L site. The above reasons led us to consider, for comparative purposes, only Ca samples. In this work we have carried out extensive studies as a function of temperature in pulsed fields up to 50 T. The samples were characterized by neutron diffraction below the charge-ordering transition temperature. Based on magnetization and neutron-diffraction data we present a systematic analysis of the phase diagrams, critical fields, and the lattice and magnetic contributions with influence in the stability of the CO phase along this paradigmatic series.

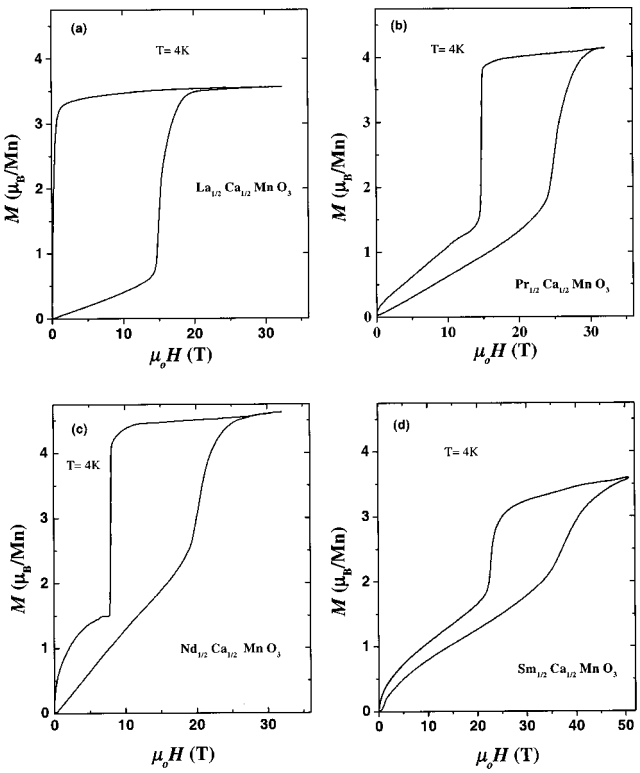

FIG. 1. Magnetization versus field curves of $L_{1/2}Ca_{1/2}MnO_3$ measured at 4.2 K. (a) La, (b) Pr, (c) Nd, and (d) Sm.

II. EXPERIMENTAL DETAILS

The measurements have been performed on polycrystalline ceramics of $L_{1/2}Ca_{1/2}MnO_3$ prepared by standard solid-state reaction in air. Sample quality was confirmed by high-resolution neutron-diffraction, magnetic, and transport measurements. High-resolution neutron diffraction (ND) measurements were performed at the Institut Laue-Langevin in Grenoble, using the D2B diffractometer ($\lambda = 1.5936$ Å) in its high flux mode. ND data of the charge-ordered phase were taken at 1.5 K. Structural and magnetic parameters were refined by the Rietveld method using the program FULLPROF.[13] The high-magnetic-field study was performed at the facilities of the SNCMP in Toulouse (France), between 4.2 and 300 K. Using the discharge of a bank capacitor in a coil, pulsed fields up to 50 T are obtained with a duration time of 0.6 s.[14]

III. RESULTS AND DISCUSSION

The magnetization measurements at 4.2 K of the perovskites with La, Pr, Nd, and Sm are shown in Fig. 1. The isothermal magnetization measurements were done after a zero-field-cooling process. In Fig. 1 the magnetization shows a sudden increase which is attributed to the melting of the CO state. Broad hysteresis loops are observed as a consequence of the energy barrier that separates melted and ordered states. Notice that there is a reduction in the steepness of the transition with small L cations. This can be ascribed to increasing lattice strain in the material as the size differences among cations at the L site increases. Within the accuracy of the high-resolution neutron-diffraction data ($\sim$3% for the oxygen occupation), we did not detect deviations in the oxygen stoichiometry. At 4.2 K the loop of $Sm_{1/2}Ca_{1/2}MnO_3$ extends over an interval of $\approx$25 T, indicating that the activation barrier between melted and CO states is very high in samples with notably tilted octahedra. Additional $M(H)$ measurements on Y and Ho samples confirmed that they show no transition to the ferromagnetic state within our available range of fields (up to 50 T).

The transition fields for the up and down sweeps (H_c^+ and H_c^-) were defined as the fields at which the highly magnetized plateau is reached (saturation fields). The temperature dependence of the large hysteretic region is characteristic of first-order phase transitions and has been discussed in detail in Ref. 2 for $Nd_{1/2}Sr_{1/2}MnO_3$.

The temperature dependence of the critical field obtained for La, Pr, Nd, and Sm has been shown in the H-T diagrams of Fig. 2. In this figure the continuous lines correspond to the evolution of the saturation fields H_c^+ and H_c^-. The dotted line represents the thermodynamic transition field H_c defined as the average of the saturation fields. Some remarks should be made about Fig. 2. First, notice that there is a positive shift in the transition field on crossing downward T_N due to the AF arrangement of Mn moments. The Néel points that are shown at zero field in Fig. 2 were determined from magnetic and ND measurements, warming the samples. The shift is not abrupt. It occurs around $\approx$190 K for La, $\approx$140 K for Pr and $\approx$125 K for Nd (for Sm is not so well-defined perhaps due to the overlap with the widening of the phase boundary at lower temperatures). It should be mentioned that the Néel point shifts upon heating and cooling runs in samples with T_{CO} not very different to T_N, as in the case of La (T_N: 155 K$\rightarrow$190 K). The shift observed in the transition fields (between 2 and 6 T) when entering the AF phase com-

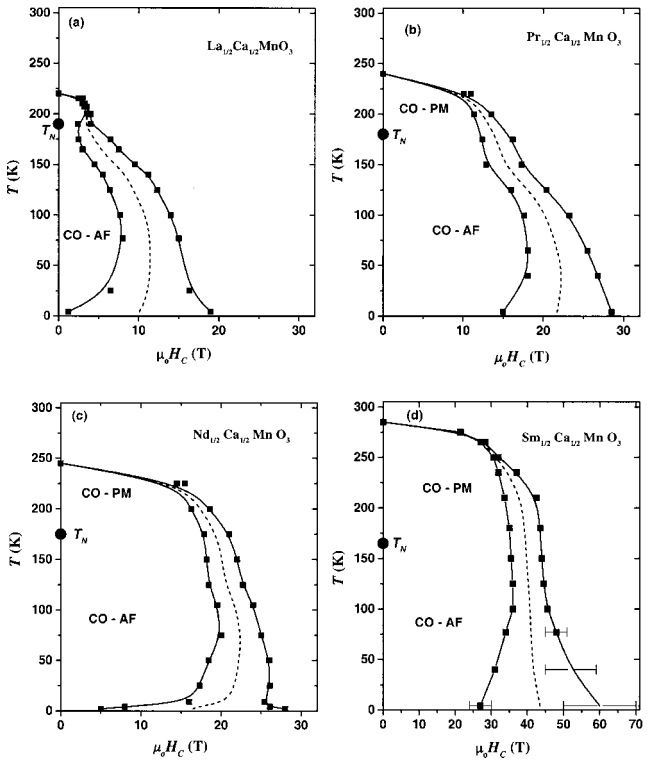

FIG. 2. *H-T* phase diagrams with the temperature dependence of the transition fields for (a) $La_{1/2}Ca_{1/2}MnO_3$, (b) $Pr_{1/2}Ca_{1/2}MnO_3$, (c) $Nd_{1/2}Ca_{1/2}MnO_3$, and (d) $Sm_{1/2}Ca_{1/2}MnO_3$. The continuous lines correspond to, respectively, the saturation fields determined for up-sweep (H_c^+) and down-sweep (H_c^-) processes. Dotted line represents the transition field H_c.

pensates for the reduced susceptibility of the AF regime.

Although the AF order occurs in $La_{1/2}Ca_{1/2}MnO_3$ coinciding with the CO transition, there is consensus that the magnetic contribution is only a very small fraction of the lattice contribution to the stability of the polaron ordering. Some arguments sustaining this are, for instance, the existence of a very broad paramagnetic CO region in the phase diagram of $Sm_{1/2}Ca_{1/2}MnO_3$ ($T_N = 165$ K versus $T_{CO} = 275$ K) or $Y_{1/2}Ca_{1/2}MnO_3$ ($T_N = 130$ K versus $T_{CO} = 260$ K). This fact agrees with the difference of 660 K between orbital and magnetic ordering in $LaMnO_3$, for instance. The extra field observable in Fig. 2 in order to melt the ordered state below the Néel point allow us to estimate the magnetic contribution to the stability of the phase. Assuming a field shift $\Delta H \approx 2(1)$ T (Pr, Nd), the extra work $\int \Delta H dM \approx 3.1 \times 10^5$ J/m^3 $= 0.40$ meV/Mn carried out by the external field in the AF phase serves to compensate the energy gain due to the CE-type AF ordering of the Mn moments. This estimation can be compared with the AF (J_c) and F (J_{ab}) exchange integrals obtained from inelastic neutron scattering in $LaMnO_3$ (0.58 and 0.83 meV, respectively).[15]

Next, we focus on the variation of the thermodynamic transition fields (H_c) determined at 4.2 K. But first we should introduce the characterization using ND of the same La, Pr, Nd, Y, and Ho samples investigated under field (Sm is too absorbent to be measured with thermal neutrons). Due to the absence of superstructure reflections in the ND patterns at 1.5 K, the *Pnma* description was used to analyze the low-temperature diffraction data. Projecting the CO phase

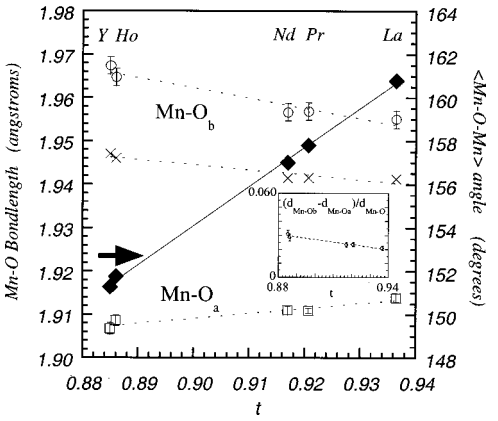

FIG. 3. Apical (Mn-O_a) and basal (Mn-O_b) bondlengths in the charge-ordered phase of $L_{1/2}Ca_{1/2}MnO_3$ (L: La, Pr, Nd, Y, and Ho) obtained from ND at 1.5 K using the orthorhombic approximation. The evolution along the series of the average Mn-O-Mn angle (1.5 K) is also shown. Inset: amplitude of stretching-type distortion mode ($\varepsilon = (d[\text{Mn-O}_b] - d[\text{Mn-O}_a])/d[\text{Mn-O}]$) at 1.5 K (averaged over the two types of octahedra in the CO phase).

over the orthorhombic symmetry, a unique MnO_6 octahedra is obtained, in which the two Mn-O(2) distances represent the same basal distance, averaged over Mn^{3+} and Mn^{4+} sites. Figure 3 shows the apical and basal bond lengths and the average $\theta = \langle \text{Mn-O-Mn} \rangle$ bond angle at 1.5 K for La, Pr, Nd, Y, and Ho samples in front of the tolerance factor ($t \equiv \langle d_{(L,A)\text{-O}} \rangle / \sqrt{2} \langle d_{\text{Mn-O}} \rangle$). The samples investigated cover a broad range of average radii ($1.069 \leqslant R_0 \leqslant 1.140$). The average angle subtended between MnO_6 octahedra changes 10° from Y to La.

In Fig. 4 we have plotted the evolution of the thermodynamic transition fields (H_c) at the lowest temperature as a function of the buckling of the Mn-O-Mn bonds. The average angle given for Sm in this figure was interpolated from the linear angular dependence displayed in Fig. 3. Figure 4

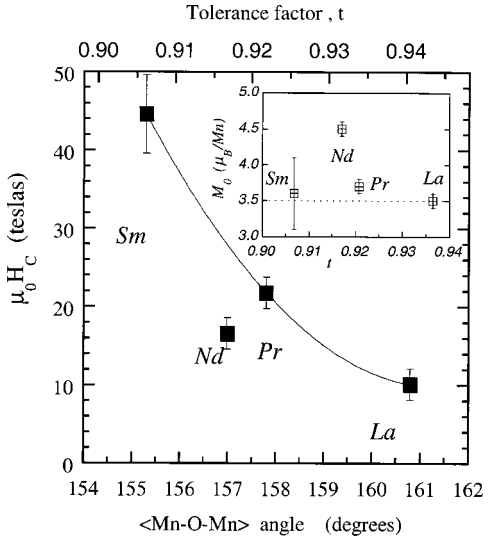

FIG. 4. Dependence of the thermodynamic critical fields H_c on the average Mn-O-Mn bond angle of the CO phase determined at 1.5 K from ND. Inset: Saturation moments M_0 obtained from magnetization measurements at 4.2 K.

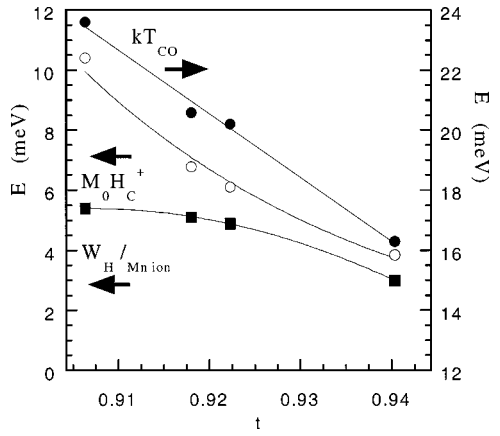

FIG. 5. Work made by the external field (W_H, closed squares) per Mn ion to collapse the charge-ordered state (sweep up process). The evolution of the Zeeman ($M_0H_c^+$ [H_c^+ at 4 K], open circles) and kT_{CO} on warming (closed circles) energies are also shown.

confirms a nonlinear H_c-θ dependence, with $|dH_c/d\theta|$ rates bigger than 7 T per degree of extra bending for lanthanides smaller than Pr. An estimate (extrapolation) of the transition field in $(Y, Ho)_{1/2}Ca_{1/2}MnO_3$ ($\theta = 151.5°$) yields $H_c \approx 84$ T, well above our maximum field of 50 T. Moreover, a simple glance over Fig. 4 reveals that $Nd_{1/2}Ca_{1/2}MnO_3$ is an exception to the general behavior of $H_c(t)$. The saturation moments M_0, obtained extrapolating to $H=0$ the magnetization data at 4.2 K of Fig. 1, are depicted in the inset of Fig. 4. Their values confirm that the resulting phase beyond the critical field is fully ferromagnetic. With Nd the external field carries out extra work in order to polarize the nonnegligible Nd moment (estimated in 2 μ_B/Nd from the inset of Fig. 4). This extra work is returned later because the internal field created by polarized Nd moments brings about a reduction of the external field required to activate the transition (27.7 T, estimated, and 17 T, experimental). On the other hand, it is worth noticing from Fig. 1(c) (Nd) that the demagnetization process takes place in two steps. During the sweep down process the magnetization after the first step suggests that, very likely, Nd moments remain polarized after the melting of the FM sublattice of Mn moments. In this interpretation, consistent with the observed excess of magnetization [see Fig. 1(c)], Nd moments gradually depolarize below 7.5 T as the applied field is progressively removed.

In Fig. 5 we have plotted the work W_H (per Mn ion) carried out by the external field during the up sweep process up to completion of the induced transition. For comparison, the Zeeman energies $M_0H_c^+$ (M_0 values given in the inset of Fig. 4 and H_c^+ taken at the lowest temperature) have been represented as well. In the case of Sm the uncertainty is large because the transition is not totally completed at 50 T (see Fig. 1). The evolution of the kT_{CO} values is included as well. $M_0H_c^+$ and W_H do not coincide in real polycrystalline systems and, as shown in Fig. 5, the difference increases when reducing the L cation size. The reason is a progressive broadening of the melting transition. Moreover, size effects are very apparent for the smallest L cations. Thus, in contrast with the pronounced rising of the transition fields, for Y charge-ordering occurs only below $T_{CO} \approx 260$ K (Ref. 16) (lower than for Sm).

The reported critical fields parameterize the CO stability in front of a magnetic field. A large CO gap (Δ_{CO}) in the density of states at the Fermi level is associated with highly stable charge-ordered state in front of electric fields. At the present, there are not parallel systematic investigations of the CO gap in 50%-doped manganites. The gap measured in $Nd_{1/2}Sr_{1/2}MnO_3$ using scanning tunneling spectroscopy was $\Delta_{CO} \approx 0.27$ eV,[16] about half of the gap found in more distorted $Y_{1/2}Ca_{1/2}MnO_3$ ($\Delta_{CO} \approx 0.5$ eV).[17] Let us finally comment on the possible factors that determine the observed evolution of the CO stability. In these Ca-doped perovskites it is assumed that $E_{JT} \gg J_{AFM}$ (E_{JT} represents the Jahn-Teller distortion energy, of typical values 0.1–0.5 eV). Competing with the E_{JT} trapping energy, the electronic kinetic energy is governed by the hybridization term $t_{eff} \sim t_0 \cos(1/2[\pi - \theta])$, with $t_0 \approx 0.7$ eV.[18] From Fig. 3 the variation of the angular contribution to t_{eff} is $\approx$2% from Y to La. Moreover, changes in the t_0 values are also expected by looking at the slight but systematic increase of the mean Mn-O distance in Fig. 3 ($\approx$0.6% along the series). The bond expansion observed could be attributed to the electronegativity increase along the $4f$ series that induces progressively more ionic Mn-O bonds. Finally, in the CO phase the difference between the measured basal [Mn-O(2)] and apical [Mn-O(1)] distances has its origin in the stretching mode that confines the occupied $d_{z^2-r^2}$ orbital in the a-c plane. Since $Mn^{4+}O_6$ octahedra are not deformed, the parameter $\varepsilon = (d[\text{Mn-O}_b] - d[\text{Mn-O}_a])/d[\text{Mn-O}]$ can be used to monitor the amplitude of the stretching-type distortion mode at the sites with one trapped e_g electron. This is done in the inset of Fig. 3. Although the E_{JT} energy is generally assumed to be constant, the figure suggests a tiny variation in the mean deformation of the octahedra that could also have some influence on the evolution of the CO stability along the $x = 1/2$ family.

To conclude, a high magnetic-field investigation of the charge-melting transition in $L_{1/2}Ca_{1/2}MnO_3$ perovskites has been presented for L:Y$\rightarrow$La. The measurements provide a systematic and detailed description of the H-T phase diagrams, critical fields, and energies involved in the melting process that have been analyzed in the light of the structural features provided by ND data.

ACKNOWLEDGMENTS

The authors would like to acknowledge financial support by the CICYT (MAT97-0699), MEC (PB97-1175), the Generalist de Catalunya (GRQ95-8029), and the TMR CEE (OXSEN) Network. Dr. J. A. Alonso is gratefully acknowledged for making available the Y and Ho samples. The ILL and SNCMP INSA laboratories are acknowledged for making available their experimental facilities.

[1] Y. Moritomo, Y. Tomioka, A. Asumitsu, Y. Tokura, and Y. Matsui, Phys. Rev. B **51**, 3297 (1995).
[2] H. Kuwahara, Y. Tomioka, A. Asamitsu, Y. Moritomo, and Y. Tokura, Science **270**, 961 (1995).
[3] S-W. Cheong, H. Y. Hwang, C. H. Chen, B. Batlogg, L. W. Rupp, and S. A. Carter, Phys. Rev. B **49**, 7088 (1994); C. H. Chen *et al.*, Phys. Rev. Lett. **71**, 2461 (1993).
[4] P. G. Radaelli, D. E. Cox, M. Marezio, and S-W. Cheong, Phys. Rev. B **55**, 3015 (1997).
[5] Y. Murakami, H. Kawada, H. Kawata, M. Tanaka, T. Arima, Y. Moritomo, and Y. Tokura, Phys. Rev. Lett. **80**, 1932 (1998).
[6] Y. Tomioka, A. Asamitsu, Y. Moritomo, H. Kuwahara, and Y. Tokura, Phys. Rev. Lett. **74**, 5108 (1995).
[7] Y. Tokura, H. Kuwahara, Y. Moritomo, Y. Tomioka, and A. Asamitsu, Phys. Rev. Lett. **76**, 3184 (1996); H. Kuwahara, Y. Tomioka, A. Asamitsu, Y. Moritomo, and Y. Tokura, Science **270**, 961 (1995).
[8] H. Kuwahara, Y. Moritomo, Y. Tomioka, A. Asamitsu, M. Kasai, R. Kumai, and Y. Tokura, Phys. Rev. B **56**, 9386 (1997).
[9] M. Tokunaga, N. Miura, Y. Tomioka, and Y. Tokura, Phys. Rev. B **57**, 5259 (1998).
[10] Y. Tomioka, A. Asamitsu, H. Kuwahara, Y. Moritomo, and Y. Tokura, Phys. Rev. B **53**, R1689 (1996).
[11] Y. Tomioka, H. Kuwahara, A. Asamitsu, T. Kimura, R. Kumai, and Y. Tokura, Physica B **246–247**, 135 (1996).
[12] H. Kawano, R. Kajimoto, H. Yoshizawa, Y. Tomioka, H. Kuwahara, and Y. Tokura, Phys. Rev. Lett. **78**, 4253 (1997).
[13] J. Rodríguez-Carvajal, Physica B **192**, 55 (1993).
[14] J. P. Lascaray *et al.*, Solid State Commun. **61**, 401 (1987).
[15] F. Moussa, M. Hennion, J. Rodríguez-Carvajal, H. Moudden, L. Pinsard, and A. Revcolevschi, Phys. Rev. B **54**, 15 149 (1996).
[16] A. Biswas, A. K. Raychaudhuri, R. Mahendiran, R. Mahesh, and C. N. R. Rao, J. Phys.: Condens. Matter **9**, L335 (1997).
[17] A. Arulraj, R. Gundakaram, A. Biswas, N. Gayathri, A. K. Raychaudhuri, and C. N. R. Rao, J. Phys.: Condens. Matter **10**, 4447 (1998).
[18] S. Ishihara, J. Inoue, and S. Maekawa, Phys. Rev. B **55**, 8280 (1997).